Machine Learning with Applications 6 (2021) 100192

Contents lists available at ScienceDirect

Machine Learning with Applications

journal homepage: www.elsevier.com/locate/mlwa

Explainable AI in drought forecasting

Abhirup Dikshit [a], Biswajeet Pradhan [a,b,c,*]

[a] Centre for Advanced Modelling and Geospatial Information Systems (CAMGIS), Faculty of Engineering and IT, University of Technology Sydney, NSW 2007, Australia

[b] Center of Excellence for Climate Change Research, King Abdulaziz University, P.O. Box 80234, Jeddah 21589, Saudi Arabia

[c] Earth Observation Center, Institute of Climate Change, Universiti Kebangsaan Malaysia, 43600 UKM, Bangi, Selangor, Malaysia

ARTICLE INFO

Keywords:
Drought forecasting
Standard precipitation index
Deep learning
Explainable AI

ABSTRACT

Droughts are one of the disastrous natural hazards which has severe impacts on agricultural production, economy, and society. One of the critical steps for effective drought management is developing a robust forecasting model and understanding how the variables affect the model outcomes. The present study forecasts SPI-12 at a lead time of 3 months, using the Long Short-Term Memory (LSTM) model, and further interprets the spatial and temporal relationship between variables and forecasting results using SHapley Additive exPlanations (SHAP). The developed model is tested in four different regions in New South Wales (NSW), Australia. SPI-12 was computed using monthly rainfall data collected from Scientific Information for Land Owners (SILO) for 1901–2018. The model was trained from 1901–2000 and tested from 2001–2018, and the performance was measured using Coefficient of Determination (R^2), Nash–Sutcliffe Efficiency (NSE) and Root-Mean-Square-Error (RMSE). To understand the underlying impact of variables on the model outcomes, SHAPley values were calculated for the entire testing period and also at three different temporal ranges, which are during the Millennium Drought (2001–2010), post drought period (2011–2018) and at a seasonal scale (summer months). The comparison of the results shows a significant variation in the impact of variables on forecasting, both temporally and spatially. It also shows the need to study the model outcomes for specific regions and for a shorter duration than the entire testing period. This is a first of its study towards interpreting the forecasting model in drought studies, which could help understand the behaviour of drought variables.

1. Introduction

The number of studies on natural hazards has increased in the 21st century, as climate change has led to the occurrence of more disastrous and frequently occurring hazards. Of all the natural hazards, one that has affected large parts of the world is drought and is expected to rise due to factors like anthropogenic activity and climate change (Van Loon, Glesson, Clark, et al., 2016). Droughts begin with a deficiency in precipitation, which then slowly propagates to a reduction in soil moisture conditions, causing agricultural drought and declines in streamflow, leading to hydrological drought and finally impacting society's social and economic aspects. Also, this may not happen chronologically, and sometimes hydrological and agricultural drought can occur simultaneously. However, it can be said that the meteorological drought will be the first step towards a chain reaction. Generally, droughts can be categorized into four types: (a) Meteorological, (b) Hydrological, (c) Agricultural, and (d) Socio-economic impacts (Mishra & Singh, 2011). Although various researchers have advocated to further categorize droughts into different drought types, like Mishra and Singh (2011) suggested to include groundwater drought; Vicente-Serrano, Quiring, Peña Gallardo, et al. (2020) urged to include environmental droughts and Slette et al. (2019) suggested ecological droughts to be a separate drought type, however, such adaptation is yet to happen.

The challenges towards understanding droughts are plenty, with the first obstacle being its definition, i.e., when does a drought start and when it ends. This challenge becomes more complicated as it is dependent on who is defining it and what metric is being used for by definition to measure it (Lloyd-Hughes, 2014). Therefore, drought indicators and indices have been developed, which would provide a general idea about droughts (Haile, Tang, Li, et al., 2020). For meteorological droughts, several researchers have defined drought indices based on different variables, and (Yihdego, Vaheddoost, & Al-Weshah, 2019) provide an extensive list of various drought indices based on drought type. Standard Precipitation Index (SPI) is one of the most used (Hayes, Svoboda, Wall, & Widhalm, 2011) drought index, one that is arguably the most popular and accepted drought index developed by McKee, Doesken, and Kleist (1993). Compared to other drought indices,

* Corresponding author at: Centre for Advanced Modelling and Geospatial Information Systems (CAMGIS), Faculty of Engineering and IT, University of Technology Sydney, NSW 2007, Australia.

E-mail addresses: abhirup.dikshit@student.uts.edu.au (A. Dikshit), biswajeet.pradhan@uts.edu.au (B. Pradhan).

https://doi.org/10.1016/j.mlwa.2021.100192
Received 19 April 2021; Received in revised form 6 October 2021; Accepted 16 October 2021
Available online 24 October 2021

it has multiple advantages, like consistent spatial interpretation, less computationally complex, which makes it suitable for prediction and risk analysis (Anshuka, van Ogtrop, & Willem Vervoort, 2019). As the calculation is exclusively based on rainfall, it has proven to be very useful in data sparse areas, where other drought affecting factors like soil moisture, streamflow etc. are unavailable (Hayes, Svoboda, Le Comte, et al., 2005).

The forecasting of meteorological drought can be carried out by either forecasting drought affecting variable (rainfall) or drought indicators (SPI) (Woli, Jones, Ingram, & Paz, 2013). The influence of atmospheric circulation patterns or teleconnections has been found to influence rainfall, thereby affecting drought occurrences (Feng, Wang, Luo, et al., 2020; Stahl & Demuth, 1999). Further, it has been well established that the future droughts would be affected, due to climatic influence; however, the inclusion of climatic indices to improve forecasting has received conflicting results. In a work by Ganguli and Reddy (2014) suggested that the addition of climatic indices improves prediction, whereas Morid, Smakhtin, and Bagherzadeh (2007) suggested it has minimal improvement in model performance.

The challenge for accurate drought forecasting lies in the length of the available time series, timescale of the drought index, and the model used. A minimum of 30 years of data is required to understand any drought characteristic. Anshuka et al. (2019) in their review article on drought forecasting using the SPI index discussed the capabilities of various models to forecast at different SPI time scales and lead times (forecast range). The study suggested that the best lead times for SPI forecasting can be found for 1–3 months. However, the selection of SPI timescale is dependent on the objectives and the drought type being studied, along with the local features such as catchment or area type, land-use changes of the study area (Vasiliades, Loukas, & Liberis, 2011), with some suggesting longer time scales to be used and the other suggesting the opposite. Their study also suggested that SPI at longer time scales are better forecasted as the values are smoother and emphasizes the need to test different time scales before integrating it in drought management. Therefore, the present study forecasts SPI12 at a lead time of 3 months.

Due to the multivariate nature of drought, modellers are often puzzled to identify which variables to use (Deo, Kisi, & Singh, 2017; Dikshit, Pradhan & Alamri, 2021; Hao, Singh, & Xia, 2018). The key finding for improving drought forecasting was the inclusion of temporal lag components of climatic indices as predictors in the model. Various studies have utilized the climatic drivers and have shown improvement in forecasting drought indices or drought variables (Abbot & Marohasy, 2014; Özger, Mishra, & Singh, 2012). This aspect becomes more critical for drought studies in Australia, where the relation between climatic drivers and rainfall is found to be the highest in the world (Kirono, Chiew, & Kent, 2010). There are several indices which depict the changes, as a single index cannot capture all the different climatic aspects (Hanley, Bourassa, O'Brien, et al., 2003). Therefore, various indices have been proposed in the literature and in the present study, we use the climatic variables (pressure indices and SST indices) described in Table 1.

The forecasting of drought events can be performed via statistical (Han, Wang, Zhang, & Zhu, 2010), physical (Pozzi, Sheffield, Stefanski, et al., 2013), and data-driven (Deo et al., 2017) approaches. The physical-based study involves complex models using several variables and high computational resources, which is quite challenging. Whereas data-driven models like machine learning models are far less complicated and use less computational resources than physical-based models. Although the use of physical-based models has led to comparable forecasting results, it has been well proven that data-driven models are more useful and can sometimes achieve even better accuracy than physical models (Abbot & Marohasy, 2014). Among the data-driven models, machine learning (ML) techniques have often been used to forecast droughts and have proven to be very successful (Deo & Şahin, 2015; Dikshit, Pradhan, & Alamri, 2020a, 2020b). Several studies have been conducted to forecast drought at different lead times using different drought indicators for various parts of the world. Interested readers can look at the important review articles by AghaKouchak, Farahmand, Melton, et al. (2015), Hao et al. (2018), Hao, Yuan, Xia, Hao, and Singh (2017), Mishra and Singh (2011). These review articles discuss the various models, variables, and the data types used in the literature to forecast drought at various spatial and temporal scales.

However, as several such variables affect different lag times, ML models succumb to the curse of dimensionality and overfitting. However, deep learning model is a new prospect and provides new possibilities towards improving forecasting capabilities. Several prominent researchers have highlighted and proved that the use of deep learning would eventually surpass ML forecasting capabilities and provide a new direction towards regression problems (Ham, Kim, & Luo, 2019; LeCun, Bengio, & Hinton, 2015; Reichstein, Camps-Valls, Stevens, et al., 2019). Such concerns of overfitting and dimensionality can be overcome by using LSTMs, wherein the forget gate determines the amount of information which can pass through (Goodfellow, Bengio, Courville, & Bengio, 2016; Olah, 2015). Although, LSTM has been often used for different fields of study, like finance, climatic studies, environmental variables, its use for forecasting drought indices/variables is in the early stages. Apart from the quest to forecast at higher lead times, the interpretation of the results in terms of lags of the variables used to forecast drought is generally not conducted in drought literature. Despite the outperformance of data-driven models, one major challenge is to interpreting the models and examining the relationships between variables and forecasting results, along with the interrelationships among the variables. Therefore, in the present study, we look towards developing a robust and explainable forecasting model and interpreting the results, which would help understand how LSTM uses the variables to forecast droughts. Previous work by Dikshit and Pradhan (2021b) showcased the importance of SHAP for drought prediction under different drought conditions. In the present study, we focus on understanding the explainable models for drought forecasting at shorter lead times, and its interaction under different time periods (annually, seasonally).

One of the most affected drought regions in the world is Australia, which is the second driest continent in the world and has suffered from several droughts (Howden, Schroeter, Crimp, & Hanigan, 2014). The present work focusses only on the south-eastern part of the country, New South Wales (NSW). The region faces synergistic pressures and stress due to change in climatic conditions leading to warmer temperatures, intensified by strong El Niño resulting in frequent to severe drought occurrences (Abbot & Marohasy, 2014; Deo et al., 2017; Dikshit & Pradhan, 2021b; Verdon-Kidd & Kiem, 2009). Drought occurrences reduce streamflow which leads to significant economic losses, especially in the agriculturally sensitive Murray–Darling Basin (MDB) (Van Dijk, Beck, Crosbie, et al., 2013). Therefore, an accurate forecasting model with the understanding of the affecting variables could help drought management and mitigate drought risk. Consequently, the present study focusses on four different regions in NSW, with two regions located inside MDB and two located along the coast. In summary, the objectives of the study are: (i) Forecast SPI 12 at a lead time of 3 months using LSTM; (ii) Interpret the forecasted models using SHAP; and (iii) Examine the interpretation results for different regions.

2. Study area

The NSW region has a long history of drought events lasting for a few months to several years. The recent Millennium Drought lasting (2001–2009) can be described as the worst drought on record for southeast Australia (Van Dijk et al., 2013). The effect of climate change has made the situation of drought even worse for NSW, which has led to an increase in drought frequency and intensity along with heatwaves, aggravating drought conditions (Cai, Purich, Cowan, van Rensch, & Weller, 2014). Dey, Lewis, Arblaster, and Abram (2019) examined the

Table 1
Description of the climatic variables used in the present study.

Climatic variable	Description
Southern Oscillation Index (SOI)	Indication of the development and intensity of El Niño or La Niña events
Pacific Decadal Oscillation (PDO)	Long-lived ENSO like pattern of Pacific climate variability
Southern Annular Mode (SAM)	Pressure diploe between the Antarctic and Southern Hemisphere mid latitudes
Indian Ocean Dipole (IOD)	SST dipole between the western and eastern tropical Indian Ocean
Nino 3.4	Mean SST over the Nino 3.4 region (5°N–5°S, 120°–170°W)
Nino 4.0	Mean SST over the Nino 4 region (5°N–5°S, 160°E–150°W)
Nino 3.0	Mean SST over the Nino 3.0 region (°5N-5°S, 150°–90°W)

Table 2
Geographic coordinates of the study sites.

Station ID	Location	Coordinates	Elevation (m)
63005	Bathurst	−33.43°S, 149.56°E	713
54003	Barraba	−30.38°S, 150.61°E	499
50031	Peak Hill	−32.72°S, 148.19°E	285
58012	Yamba	−29.43°S, 153.36°E	27.4

historical rainfall changes and observed a decrease in mean rainfall since 1950. The present study focuses on four different regions (Fig. 1), Barraba, Bathurst, Peak Hill and Yamba. Of these, Barraba and Bathurst are situated within MDB, and the other two (Peak Hill and Yamba) are situated in the coastal part of the state. (See Table 2)

The variation in rainfall patterns in NSW has been found to be linked to the climatic drivers arising from the Pacific Ocean, Indian Ocean, and the Southern Ocean. The changes arising due to the Pacific Ocean are known as El Niño/Southern Oscillation (ENSO) and Pacific Decadal Oscillation (PDO). The understanding of the ENSO phase is defined using an index, based either on SST or atmospheric changes (Hanley et al., 2003). The presence of a single index accurately defining ENSO is currently lacking (Huang, L'Heureux, Lawrimore, et al., 2013). The SST based indices influencing NSW are Niño3.0, Niño3.4 and Niño4.0, and the atmospheric based index is the Southern Oscillation Index (SOI) (ESRL Earth System Research Laboratory, 2020). The anomalies arising in the Southern Ocean are called as Southern Annular Mode (SAM), and from the Indian Ocean is Indian Ocean Dipole (IOD). Droughts in the region have been traditionally linked to ENSO events (Nicholls, Lavery, & Frederiksen, 1996). However, Ummenhofer, England, McIntosh, et al. (2009) found that IOD variations majorly drove the Millennium Drought. This shows that climatic drivers do affect droughts, and the future drought events would be affected due to these changes.

As drought occurrence is a resultant of a multitude of reasons, we chose 8 different variables that influence droughts in the region as predictors in the model (Deo et al., 2017). These include the meteorological parameters, climatic indices and the sea surface temperatures (SSTs). The data for the meteorological parameters were collected from Scientific Information for Land Owners (SILO). The data was collected from 1901–2018, of which 85% (1901–2000) was used to train the model, and the remaining was used as a testing period.

2.1. Standard precipitation index

SPI was conceptualized by McKee et al. (1993), which involves fitting a gamma probability density function for the distribution of monthly precipitation data at different time scales. The classification of droughts based on the index values representing various drought conditions is depicted in Table 3 (Morid et al., 2007). The detailed understanding of the calculation of the SPI index has been explained in Belayneh, Adamowski, Khalil, and Ozga-Zielinski (2014) and Deo et al. (2017). SPI is determined by fitting the probability distribution and transforming to a normal distribution, to achieve the mean value of zero (Naumann, Barbosa, Carrao, Singleton, & Vogt, 2012). It can be computed for various time series (1, 3, 6, 9, 12, 24 months), which depict different drought types. The calculation of SPI values is dependent on the choice of the probability density function $f(R)$ of

Table 3
Drought classification according to SPI definition (Morid et al., 2007).

SPI values	Drought categories
≤ −2	Extremely dry
−1.99~−1.5	Severely dry
−1.49~−1	Moderately dry
−0.99~0.99	Near normal
1~1.49	Moderately wet
1.5~1.99	Severely wet
≥ 2	Extremely wet

rainfall (R). We used the gamma probability density function, which has been majorly used (Deo et al., 2017) and can be defined as:

$$f(R) = \frac{1}{\beta^{\alpha}\tau(\alpha)} R^{\alpha-1} e^{\frac{-x}{\beta}} \quad (1)$$

where, parameters, α and β can be estimated using maximum likelihood solution; $\alpha = \frac{1}{4A}(1+\sqrt{\frac{1+4A}{3}})$; $\beta = \frac{\alpha}{\overline{R}}$, where $A = \ln\left(\overline{R}\right) - (\sum \ln(R))/M$; and M is the number of rainfall observation months.

The positive and negative values depict higher and lower mean precipitation, respectively. The drought event initiates when the value reaches −1 and terminates upon reaching positive value (Morid, Smakhtin, & Moghaddasi, 2006). The calculation of the index was carried out in 'R' software using the available packages. The present study determines SPI values at a time scale of 12 months.

Fig. 2, illustrates different drought characteristics like drought onset, end, intensity. The figure depicts SPI-12 values for Bathurst Agricultural Station during the Millennium Drought from January 2001 to December 2010. As per the running sum technique (Yevjevich, 1967), the drought onset begins with the SPI value moves towards negative values and ceases when the value moves towards positive value. As seen in Fig. 2, a dip in rainfall values leads to a drop in SPI values, and drought duration can be determined by the accumulation of consecutive months, suggesting negative SPI values with peak intensity being the minimum SPI value.

3. Models

3.1. Basics of LSTM architecture

Fig. 3 illustrates the LSTM structure wherein a cell is the basic building block and its state is the key to the model. The cell states can be determined by three gates types: (i) input, (ii) forget; and (iii) output gate. Essentially, the input gate determines whether to allow including new inputs, the forget gate decides whether to discard currently used information as it may or may not be important anymore, and the output gate controls the amount of information that needs to pass through.

The details of the LSTM architecture can be found in Dikshit, Pradhan and Huete (2021) wherein the authors have used the same approach to forecast monthly SPEI for New South Wales. However, due to the change in the input data, the architecture used in the present study was slightly modified. In general, the LSTM architecture consisted of an input layer, one LSTM layer and dense layer (also known as fully connected layers). The input of the whole network is in 3D tensor form, which is the sample size, sequence length and the number of features.

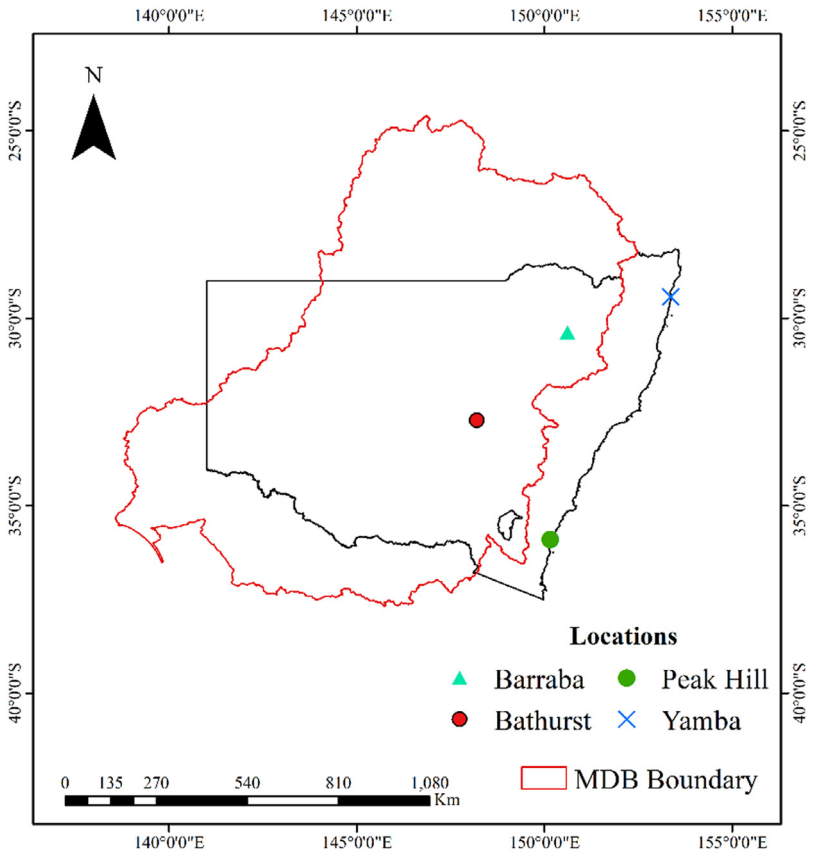

Fig. 1. Location of the Murray–Darling Basin (MDB) and four studied regions in NSW.

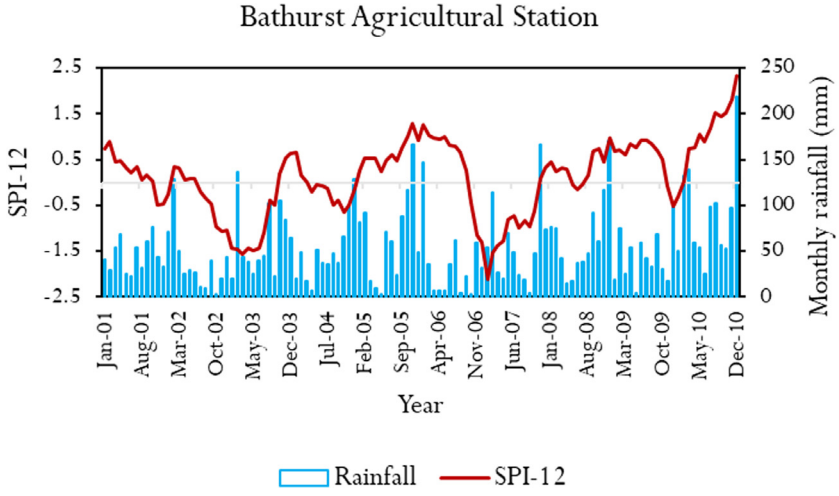

Fig. 2. SPI-12 during the Millennium Drought (2001–2010) for Bathurst Agricultural station.

Sample size equals the training dataset, which in this case is from 1901–2000. The sequence length is the temporal size of the input data which would be used to forecast SPI-12, and herein the best sequence length was found to be 12. In simple terms, the last 12 months' value of the variables is used to forecast the 13th month's SPI-12.

To forecast at longer lead times, two approaches are usually used, (i) recursive approach and (ii) direct approach. In case of recursive approach, the parameters of the sequence length are used to forecast the first monthly step, and thereafter the forecasted result is used to determine the values of the next time step. For a direct approach, the parameters of the previous time steps are used to forecast ahead at all lead times. Mishra and Desai (2006) forecasted SPI using Artificial Neural Network (ANN) in Kansabati river basin, India and examined both the approaches. Their study found that forecasting at higher lead times using a direct approach produced better results instead of a recursive based approach. Therefore, in this study, we used a direct based approach. To prevent overfitting, a dropout layer is added post LSTM layer and is empirically set to 0.25 (Dikshit, Pradhan & Huete, 2021). The number of neurons in the LSTM layer was 200, and 8 in the dense layer. The number of features was 8, and was implemented with Keras using GPU TensorFlow 2.0 as the backend (Francois, 2015). Fig. 3 depicts the flowchart used in the present study and a general representation of the LSTM architecture.

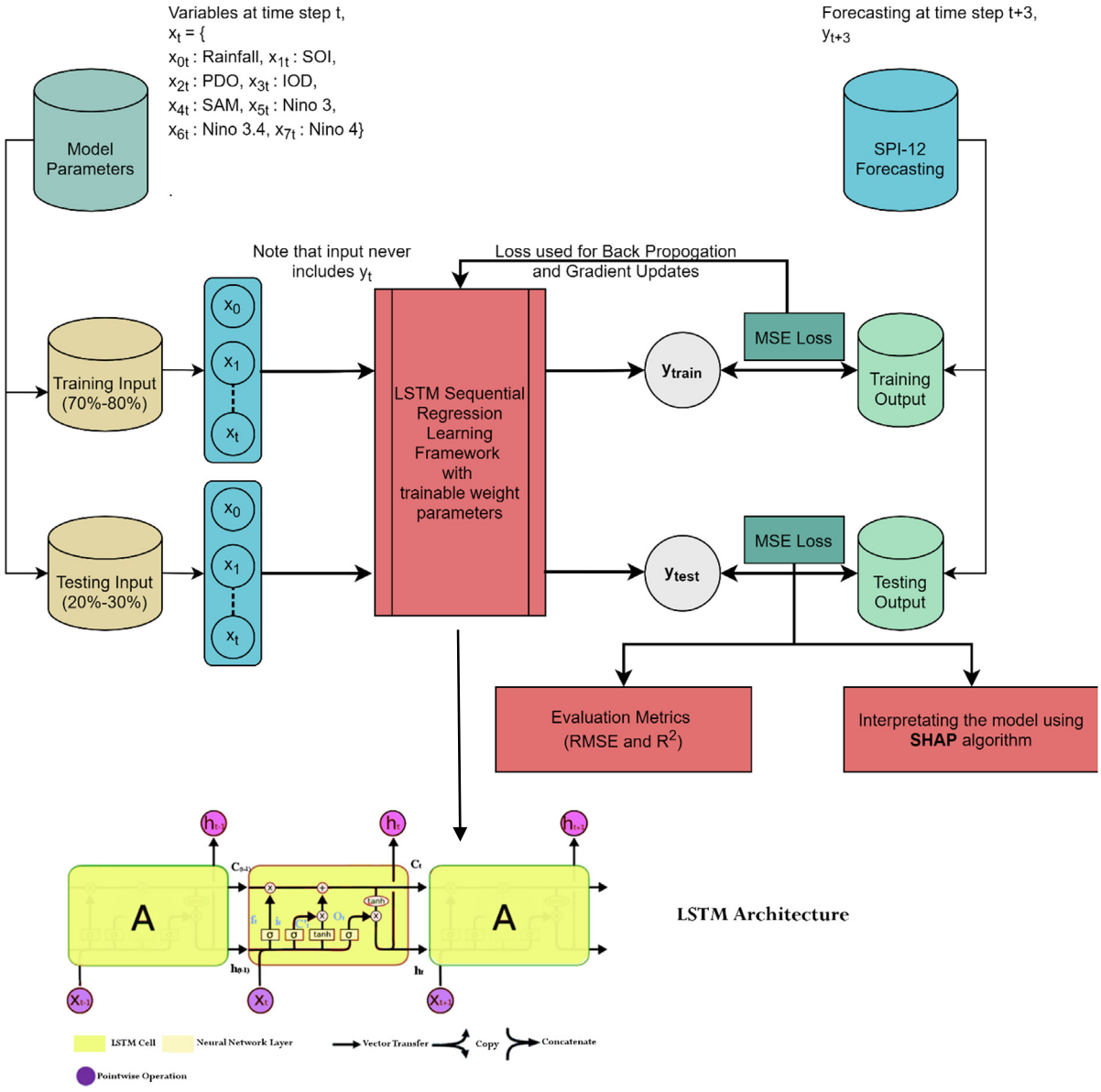

Fig. 3. Methodology adopted in the present study.

The activation function used for all the station data was 'sigmoid'; the loss function used was 'Mean Square Error (mse)' and the optimizer used was Adam. These aspects are crucial, as changing it may yield to different results (Dikshit, Pradhan & Huete, 2021). In several experiments, especially on loss and activation function, we found that this architecture involving the number of neurons and sequence length performed the best. Although one can argue that the use of Stacked LSTM (multiple LSTM layers), or a hybrid LSTM architecture would have provided better results, it is important to note that the primary objective of the study is to introduce SHAP algorithm for drought forecasting as a way to explain the model outcomes. At present, the explainable models (SHAP) have not been developed enough to decipher complex architectures.

3.2. SHAP methodology

The SHapley Additive exPlanations value (SHAP) algorithm was originally developed as a concept in game theory to determine an individual player's contribution to a collaborative game (Lundberg & Lee, 2017; Ribeiro, Singh, & Guestrin, 2016; Shapley, 1953). In game theory, this concept was applied to determine the importance of a single player in a collaborative team game. The idea was to distribute the total gain among players based on their contributions towards the outcome. The SHAP values provided a solution to the problem of a fair reward to every player and assigning a unique value determined by local accuracy, consistency, and null effect (Shapley, 1953).

The Shapley values estimate both the magnitude and the direction of each feature towards the model's outcomes. Positive indicates more contribution in the right direction and negative indicates contribution in the opposite direction towards achieving the prediction outcomes.

In particular, the importance of a feature i is defined by the Shapley value in Eq. (2):

$$\emptyset_i = \sum_{S \subseteq N \setminus \{i\}} \frac{|S|!\,(n - |S| - 1)!}{n!} \left[v(S \cup \{i\}) - v(S) \right] \tag{2}$$

where, $\emptyset\_i$ is the contribution of feature i, N is the set of all the features, n is the number of features in N, S is the subset of N which contains the feature i and v (N) is the base value meaning the predicted outcome for each feature in N without knowing the feature values.

SHAP provides multiple explainers for different AI based models: (i) Tree Explainer (e.g. — XGBoost); (ii) Kernel Explainer (e.g. — Random

Table 4
Statistical metrics of the forecasted results at different locations.

Location	RMSE	R^2	NSE
Bathurst	0.252	0.921	0.906
Barraba	0.253	0.918	0.884
Yamba	0.302	0.901	0.862
Peak Hill	0.279	0.911	0.879

Forest); (iii) Gradient Explainer and (iv) Deep Explainer (Christoph, 2019). Using the relevant explainer, four different types of interpretation can be conducted, which are: (i) Summary Plot; (ii) Dependence Plot; (iii) Individual Force Plot; and (iv) Collective force plot. The summary plot explains the relative importance of each variable on the model outcome. The dependence plot explains the effect a single feature has on the predictions made by the model. The individual force plot explains the effect of a single feature affecting positively or negatively towards the model results. The collective force plot is similar to individual force plot, with the only change being adding all the features in a single diagram. Although, there are several types of plot, readers are referred to Christoph (2019) for an in-depth detail.

4. Results

This section presents the forecasted results using the LSTM architecture and the various plots generated using the SHAP algorithm. The statistical metrics used for analysing model performance are the coefficient of determination (R^2), Nash–Sutcliffe Efficiency (NSE) and the root-mean-square-error (RMSE) method (Chai & Draxler, 2014; Dikshit, Pradhan, & Alamri, 2020c; Krause, Boyle, & Bäse, 2005; Nash & Sutcliffe, 1970). RMSE is frequently used as a metric, as it penalizes large errors and is suitable for forecasting purposes (Dikshit, Pradhan & Huete, 2021). R^2 ranges from 0 to 1, where 1 depicts an exact match, and 0 denotes no association. Contrarily, a lower RMSE value illustrates better performance. The mathematical equation of these metrics are given in Eqs. (3)–(5):

$$R^2 = \left(\frac{\sum_{i=1}^{n} \left(SPI_o - \overline{SPI}_F \right) \left(SPI_F - \overline{SPI}_F \right)}{\sqrt{\sum_{i=1}^{n} \left(SPI_o - \overline{SPI}_F \right)^2} \sqrt{\sum_{i=1}^{n} \left(SPI_F - \overline{SPI}_F \right)^2}} \right)^2 \tag{3}$$

$$RMSE = \sqrt{\sum_{i=1}^{n} \frac{(SPI_o - SPI_F)^2}{n}} \tag{4}$$

$$NSE = 1 - \frac{\sum_{i=1}^{n} (SPI_o - SPI_F)^2}{\sum_{i=1}^{n} (SPI_o - \overline{SPI}_o)^2} \tag{5}$$

where, SPI_o and SPI_F are observed and forecasted values, with $\overline{SPI}_o$ and $\overline{SPI}_F$ are the mean of the observed and forecasted observations, and n being the number of data points. Table 4 presents the forecasted results in terms of statistical metrics, and Fig. 4 depicts the plots between the actual and the forecasted results.

The advantage of using LSTM over conventional machine learning models is that it learns variable weights across time steps, unlike learning uniform weights in the latter case. As anomalies exist among the variables, decay over weights across time periods is necessary (Dikshit, Pradhan & Huete, 2021). The forget gate in a LSTM architecture captures the decay weighted lag–lead sequence relationship effectively without the vanishing gradient issue, thereby affirming its use over conventional neural networks architectures.

4.1. Summary plot

As expected, Fig. 5 shows rainfall to be the most important factor. For all the locations, Niño4 plays the second most important factor, post that there is no clear trend, and as we go from top to bottom, the bottom half becomes less significant based on the mean SHAP values.

Previous researches on drought forecasting in the region has also shown Niño indices playing a key role. As an example, Feng et al. (2020) used a machine learning algorithm, Random Forest, to forecast monthly SPI and found Niño3.4 to be the most important factor. However, it is important to note that not all the locations show the same variable significance and the actual mean values of SHAP are minimal. As and when higher lead times are forecasted, these indices would play a more important role, thereby increasing their mean SHAP values. Such variable importance plots can also be illustrated using different machine learning models. However, the interaction among the variables is not discussed in the literature, and thereby, the next section would look at the dependence plot feature of the SHAP algorithm.

4.2. Dependence plot

The understanding of the interdependence of the variables affecting the forecasting results has long been a challenge among researchers. The dependence plot feature in SHAP can help in understanding the dependence of all the variables in forecasting SPI-12. The 8 variables included in the forecasting model, would lead to a total of 56 plots. Herein, we present (Fig. 6) the relationship among the two most important variables for all the locations, during the testing period.

Fig. 6 illustrates the dependence plots among the two most important variables during the testing period, with the left coordinate axis representing the SHAP values, the right coordinate axis representing the Niño4, abscissa representing the rainfall values and the colour ranging from blue to pink showing importance from low to high. In general, a monthly rainfall of more than 100 mm, increases the prediction results, and when it is less than 100 mm, there is no clear trend and depends on the location and Niño4. As an example, in the case of Bathurst, there is no linear trend, which is the same in the case of Peak Hill and Yamba. The spread in these plots suggests that other variables must interact with rainfall. However, in case of Barraba, a low rainfall with high Niño4 values increases the model predictions. Such critical analysis can be performed among all the variables, however, when looking at the SHAP values of the summary plot, the first 2 variables (Bathurst and Peak Hill) or first 3 variables (Barraba and Yamba) were the most critical.

Although these plots can prove to be useful, they do not explain how the variables affect the model results at different temporal ranges. Hence, to better examine the effect of variables on model results, we developed 3 different dependent plots, representing different temporal ranges. These two different temporal ranges are: (i) during the Millennium Drought (2001–2010); (ii) after the Millennium Drought (2011–2018); and (ii) seasonal scale, to understand the temporal variation in a particular season (herein, we provide only the summer months, December–January–February (DJF). Such in-depth analysis would help in understanding how the interaction of variables affects the model results at various stages of the testing period.

4.2.1. Temporal based dependent plots

When examining the dependence plots under different temporal ranges, it provides contrasting results. Fig. 7 depicts the dependence plots between rainfall and Niño4 at three different temporal ranges for all the locations, with the axis being similar to Fig. 6.

The summary plots above depict the interaction of the rainfall and Niño4 in predicting the SPI-12 value. Although at the first glance all the plots show an upward trend depicting the positive impact of rainfall on SPI, the spread in the plot suggests that the other variable must interact with SPI prediction. For example, in all the plots when the rainfall is less than 100 mm, there are many observations with similar rainfall that both decrease and increase the prediction. Therefore, higher SHAP rainfall values indicate monthly rainfall of more than 100 mm.

Fig. 4. Variation between the actual and the forecasted results at different locations.

Although the effect of Niño4 compared to other climatic variables was more prominent, and therefore we restrict ourselves to examine the interrelationship only among these variables. Herein, we analysed the various scenarios which affect the model results either positively or negatively. Higher rainfall values indicate monthly rainfall of more than 100 mm, whereas higher Niño4 values indicate values more than 0.25.

During the Millennium Drought (2001–2010), the distribution of the pink dots suggests that, when rainfall is less than 100 mm, generally there are many observations where higher Niño4 values in Barraba and Peak Hill leads to a decrease in the prediction results. Whereas, the effect of lower Niño4 values in both these regions was not predictable as the observations are scattered (blue points) with some positively affecting the model outcome and some negatively affecting the model outcomes. Whereas, for Bathurst and Yamba region, most of the low Niño4 values increased the prediction results and high Niño4 values behaved differently and therefore, the general trend cannot be seen.

After the Millennium Drought (2011–2018), most Niño4 observations with lower Niño4 values increased the forecasting results, while most of the higher value observations behaved unpredictably in impacting on the forecasting results in Yamba and Bathurst. In case of Barraba and Peak Hill, the random distribution of the pink and blue dots indicates that the effect of Niño4 is unpredictable irrespective of it being high or low.

Furthermore, when analysing from a seasonal point of view, i.e., the summer season (DJF), the majority of higher Niño4 values decreased the prediction results in Barraba and Peak Hill and disperse distribution of lower value indicates that these observations can decrease or increase the prediction. For Yamba, most of the higher Niño4 values (pink dots), increased the forecasting results and were not predictable in case of average values (purple points) and lower values (blue points). However, for Bathurst, the majority of the lower Niño4 observations improved the model results and were neutral for higher Niño4 values.

As the figures show, the dependence among the variables affecting the model's results varies spatially and temporally. Such examination provides evidence in understanding the effect of climatic indices on forecasting results. It is important to note that this is a preliminary study suggesting the use of explainable models towards forecasting drought, and more in-depth analysis can also be done for forecasting at higher lead times.

5. Discussions

The inclusion of climatic variables has been found to improve the forecasting results using data-driven models for longer lead times. However, with the inclusion of several variables, involving lag components, neural networks often succumb to overfitting. The use of interpretable AI could not only help to explain the model outcomes but also for selecting important features, thereby building a more efficient and

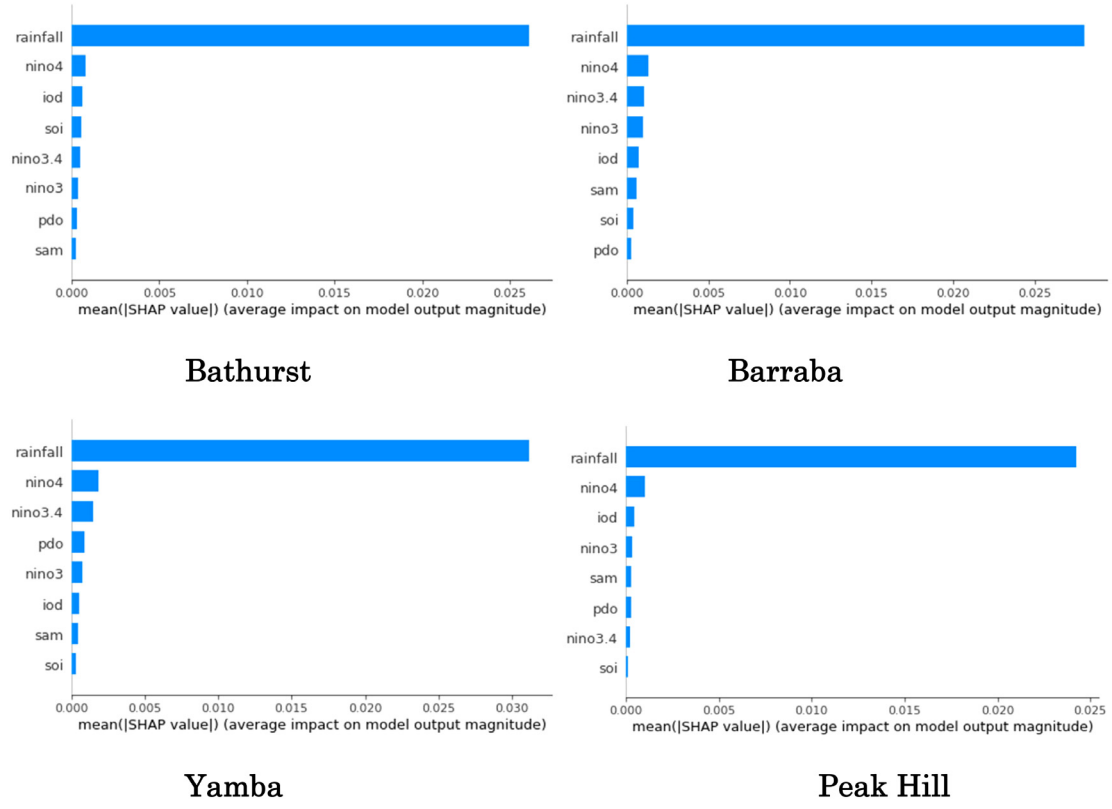

Fig. 5. Summary plots illustrating the variable importance at different locations using LSTM for SPI-12 forecasting at lead times of 3 months.

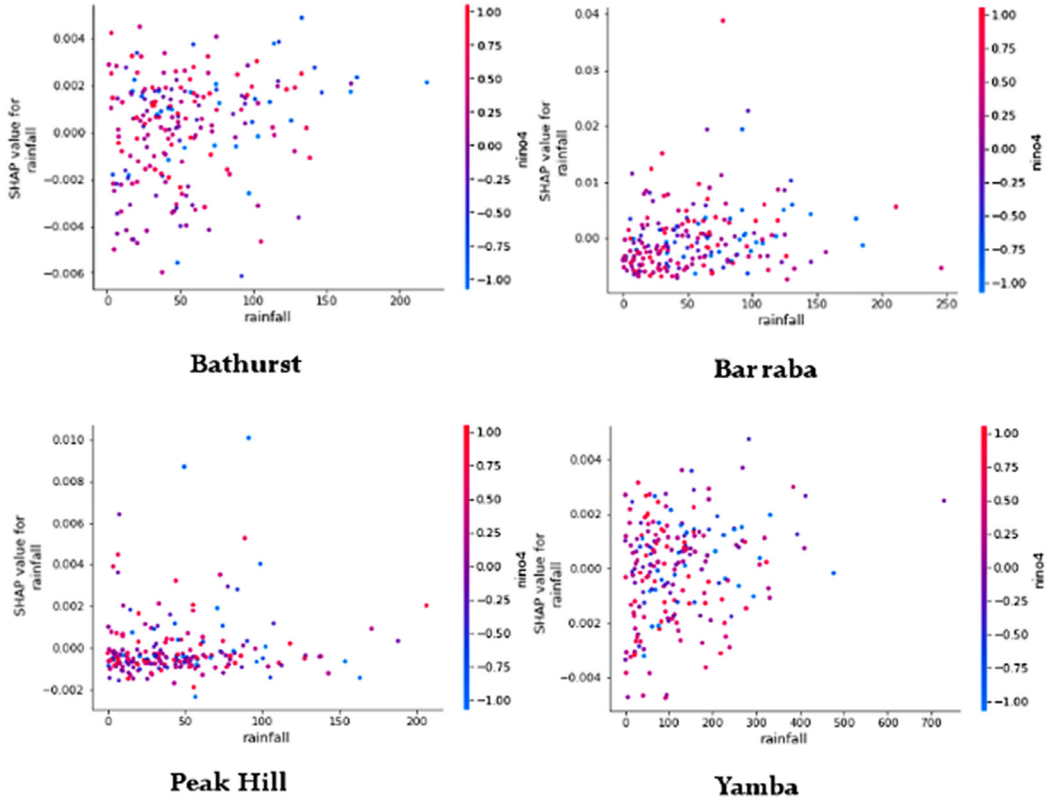

Fig. 6. Dependence plots between the two most important variables during the testing period. (For interpretation of the references to colour in this figure legend, the reader is referred to the web version of this article.)

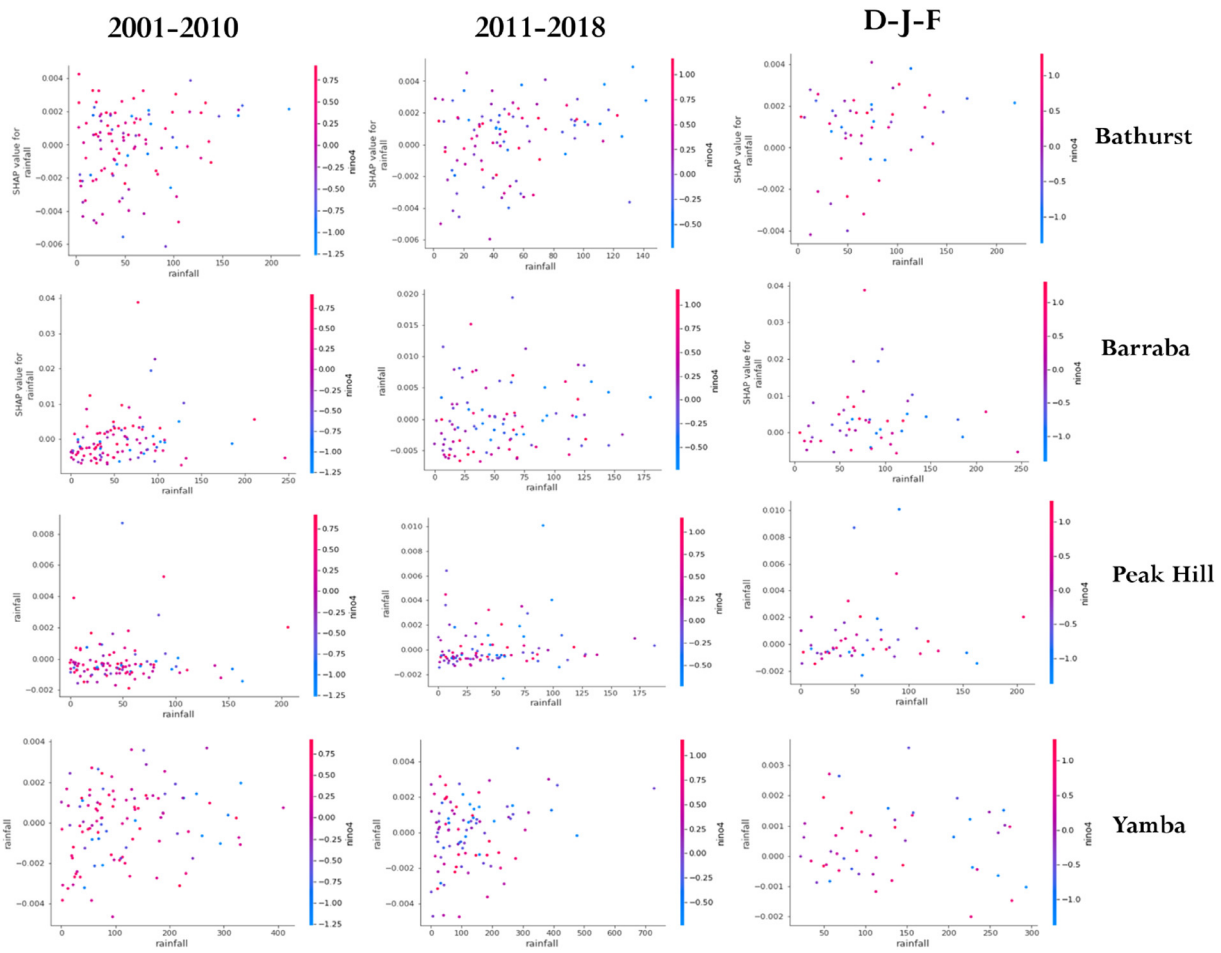

Fig. 7. Dependent plots between rainfall and Niño4 at different temporal ranges (during the drought (2001–2010), after the drought (2011–2018) and summer season (2001–2018) from left to right) for all the four locations.

robust model. The present study analyses the model outcomes, which were carried out for 4 different regions of New South Wales, of which two were situated in the agriculturally sensitive MDB region and two were located near the coast. Further, the emphasis of this study is on analysing the importance of individual features using SHAP to have a better understanding of the variables' impacts on the model outcome.

A deep learning RNN-based approach, LSTM was used to forecast SPI-12, which was trained on 100 years of data (from 1901 to 2000) and 18 years of data (from 2001 to 2018) was used to test the model. The model used 7 different climatological variables to forecast SPI-12 at a lead time of 3 months. The performance of the model showed R^2 value more than 0.9 in all the regions. Although the use of hybrid models can lead to better forecasting results, the primary objective of the article is to introduce SHAP in the field of drought forecasting. SHAP algorithm provides multiple plots which help to identify the importance and dependence of the variables on the model outcome.

For example, the SHAP summary plot, which ranks features based on their impact on the model result shows that Niño4 is the most important feature in the model after rainfall. Deo et al. (2017) used different machine learning models to forecast monthly SPI highlighted the importance of lagged Niño indices for better accuracy in forecasting results. Feng et al. (2020) forecasted SPI-8 using the Random Forests model for the Australian wheat belt region and found Niño3.4 to be the dominant climatic variable. Power, Delage, Chung, Ye, and Murphy (2017) show that a nonlinear relationship exists between rainfall anomalies and ENSO events. The low raking of IOD and SAM variables can stem from the fact that it majorly affects rainfall in Western Australia (Feng et al., 2020), and therefore is less likely to influence SPI in the studied area (Risbey, Pook, McIntosh, et al., 2009).

Although, it has been well-proven that adding lagged climatological variables increases the accuracy of the drought forecasting model, there is no study that shows how these variables are interacting individually to affect the model outcome. To explore this interaction, we plot SHAP dependence plots among the two most important variables (rainfall and Niño4 in this case) for all the regions, with rainfall on the x-axis and the SHAP value of it on the Y-axis by changing Niño4 in this model. These dependant interactions were initially plotted for the entire testing period. The result (Fig. 6) shows that when the rainfall is approximately more than 100 mm, the trend of the observations is upward (higher SHAP rainfall values), suggesting that it increases the forecasting. However, due to the dispersion of the observations, such clear demarcation was not present when monthly rainfall was less than 100 mm. Therefore, we divided the dependence plots at shorter meaningful temporal periods to take full advantage of the information hidden in temporal trends. Hence, we divided the dependence plots at three different temporal ranges, the first two being during and post the Millennium Drought and the third being only the summer months (D–J–F) for the entire testing period.

As shown in Fig. 7, this division into temporal ranges provided a more clear depiction of how the variables affected the model outcomes at different locations. Fig. 8 provides a summary of the model effects on forecasting results, in terms of increasing and decreasing effect on model results. Blue colour shows an increase in model outcomes, whereas the orange colour shows a decrease in outcomes.

The analysis shows different scenarios where climatic indices impact the model outcomes, with Niño4 impacting the results at every temporal range. As illustrated in the above figure, the blue colour is

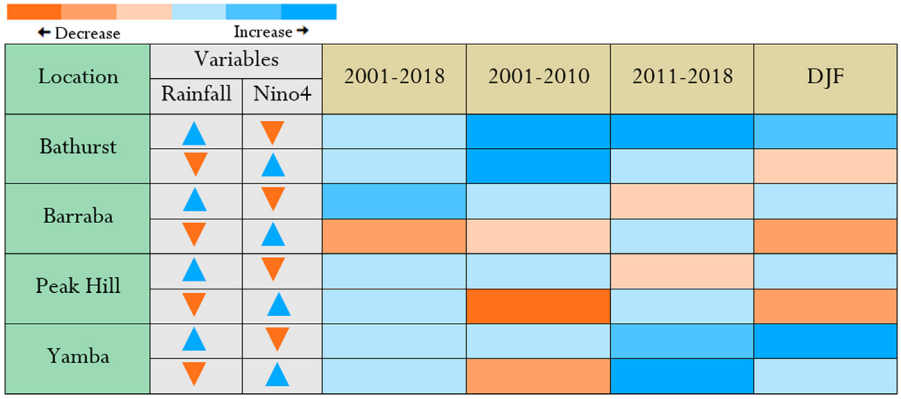

Fig. 8. Evident trends on the model results at different temporal ranges for all the locations. (For interpretation of the references to colour in this figure legend, the reader is referred to the web version of this article.)

dominant in the majority of the cases, with some cases reflecting a negative impact. This also shows that the involvement of climatic variables affects differently at different regions. When comparing spatially between the coastal and basin areas, a clear pattern indicating similar changes was not observed. As it was explained, such results were not possible if the analysis was limited to investigate the interaction of the variables in the entire testing period. Therefore, in order to better understand the outcome of the drought forecasting model, it is important to analyse the results for a shorter duration. Such an analysis could help to understand how the effect of variables affects the model results at different time frames and understand the temporal trends. Future studies should look towards using an explainable algorithm to not only examine the model outcomes but also for feature selection, thus enabling more transparency in the use of neural networks for drought forecasting.

6. Conclusions

Droughts are one of the most complex natural hazards owing to a variety of factors, including climatological and climatic variables. However, one characteristic of droughts which makes it different from other hazards is the longer timeframe it takes to have a significant impact on socio-economic aspects. This gives researchers time to focus on forecasting aspects, which would help in understanding the different phases of drought. Here, we focus on forecasting meteorological drought (SPI-12) for four different regions in NSW of Australia, at a lead time of 3 months. The choice of the index was based on two reasons; (i) Literature suggested that SPI-12 was a good indicator for droughts in NSW (Dikshit & Pradhan, 2021a); and (ii) SPI at longer time scales can be better forecasted due to smoother values compared to SPI at shorter time scales (Anshuka et al., 2019). Although the research on drought forecasting has seen the use of several data-driven models resulting in high forecasting accuracy, the interpretability of the models is yet to be conducted. Therefore, the primary objective of the article was to examine the relationships between drought affecting variables and forecasting results. Also, we analysed the interrelationships between variables and how it affects the forecasting. The study uses a deep learning approach, namely, Long Short Term Memory (LSTM) model to forecast SPI-12 and SHAP to interpret the model. The input data was collected from SILO and divided into two parts, training (1901–2000), and testing (2001–2018). The findings from the study can be summarized as:

1. LSTM can be used as a useful architecture to forecast droughts, which leads to R^2 value of more than 0.9.
2. The use of SHAP helps understand how climatic indices affect the model results. The summary plot depicts the most important variables, which were rainfall and Niño4. The SHAP dependent plots demonstrated how the inclusion of climatic variables improved the forecasting results. The results indicated that for a monthly rainfall of less than 100 mm, it improved the forecasting results.
3. Although, the dependent plots provide a relative understanding of the variable impact, breaking it into different temporal ranges leads to a more clear understanding of how the variables effect various time periods.

The use of Deep Explainer in SHAP algorithm is still in its infancy. The present work suggests that it could prove to be useful to understand the relationships among the variables, in drought forecasting. Future works would look towards the use of SHAP for long lead time drought forecasting and improving the algorithm to handle the raster datasets, which would help examine the spatial variation of the variables.

CRediT authorship contribution statement

Abhirup Dikshit: Conceptualization, Methodology, Modelling, Writing - original draft. **Biswajeet Pradhan:** Conceptualization, Supervision, Validation, Visualization, Writing - review & editing, Funding acquisition.

Declaration of competing interest

The authors declare that they have no known competing financial interests or personal relationships that could have appeared to influence the work reported in this paper.

Acknowledgements

The authors are thankful to the Scientific Information for Land Owners (SILO) for providing the rainfall data. We also thank Sahar Soleimanimatin, UTS for her analytical insights on interpreting the SHapley results. The study was supported by the Centre for Advanced Modelling and Geospatial Information Systems (CAMGIS), Faculty of Engineering & IT, University of Technology Sydney. A.D. was supported by the IRTP scholarship funded by the Department of Education and Training, Govt. of Australia.

References

Abbot, J., & Marohasy, J. (2014). Input selection and optimisation for monthly rainfall forecasting in Queensland, Australia, using artificial neural networks. *Atmospheric Research*, *138*, 166–178.

AghaKouchak, A., Farahmand, A., Melton, F. S., et al. (2015). Remote sensing of drought: progress, challenges and opportunities. *Reviews of Geophysics*, *53*, 452–480.

Anshuka, A., van Ogtrop, F. F., & Willem Vervoort, R. (2019). Drought forecasting through statistical models using standardised precipitation index: A systematic review and meta-regression analysis. *Natural Hazards*, *97*, 955–977.

Belayneh, A., Adamowski, J., Khalil, B., & Ozga-Zielinski, B. (2014). Long-term SPI drought forecasting in the Awash River Basin in Ethiopia using wavelet neural network and wavelet support vector regression models. *Journal of Hydrology*, *508*, 418–429.

Cai, W., Purich, A., Cowan, T., van Rensch, P., & Weller, E. (2014). Did climate change-induced rainfall trends contribute to the Australian millennium drought. *Journal of Climate*, *27*, 3145–3168.

Chai, T., & Draxler, R. R. (2014). Root mean square error (RMSE) or mean absolute error (MAE)? Arguments against avoiding RMSE in the literature. *Geoscientific Model Development*, *7*, 1247–1250.

Christoph, M. (2019). Interpretable machine learning. A guide for making black box models explainable. https://christophm.github.io/interpretable-ml-book/.

Deo, R. C., & Şahin, M. (2015). Application of the artificial neural network model for prediction of monthly standardized precipitation and evapotranspiration index using hydrometeorological parameters and climate indices in eastern Australia. *Atmospheric Research*, *161–162*, 65–81.

Deo, R. C., Kisi, K., & Singh, V. P. (2017). Drought forecasting in eastern Australia using multivariate adaptive regression spline, least square support vector machine and M5Tree model. *Atmospheric Research*, *184*, 149–175.

Dey, R., Lewis, S. C., Arblaster, J. M., & Abram, N. J. (2019). A review of past and projected changes in australia's rainfall. *WIREs Climate Change*, *10*, e577. http://dx.doi.org/10.1002/wcc.577.

Dikshit, A., & Pradhan, B. (2021a). Agricultural drought variation under different climatic datasets for New South Wales, Australia. In *43rd COSPAR scientific assembly*: *Vol. 43*, (p. 113).

Dikshit, A., & Pradhan, B. (2021b). Interpretable and explainable AI (XAI) model for spatial drought prediction. *Science of the Total Environment*, *801*, Article 149797.

Dikshit, A., Pradhan, B., & Alamri, A. M. (2020a). Pathways and challenges of the application of artificial intelligence to geohazards modelling. *Gondwana Research*, http://dx.doi.org/10.1016/j.gr.2020.08.007.

Dikshit, A., Pradhan, B., & Alamri, A. M. (2020b). Short-term spatio-temporal drought forecasting using random forests model at New South Wales, australia. *Applied Sciences*, *10*(4254).

Dikshit, A., Pradhan, B., & Alamri, A. M. (2020c). Temporal hydrological drought index forecasting for New South Wales, Australia using machine learning approaches. *Atmosphere*, *11*, 585.

Dikshit, A., Pradhan, B., & Alamri, A. M. (2021). Long lead time drought forecasting using lagged climate variables and a stacked long short-term memory model. *Science of the Total Environment*, *755*(2), Article 142638.

Dikshit, A., Pradhan, B., & Huete, A. (2021). An improved SPEI drought forecasting approach using the long short-term memory neural network. *Journal of Environmental Management*, *283*, Article 111979.

ESRL Earth System Research Laboratory (2020). National Oceanic and Atmospheric Administration. Available at: https://www.esrl.noaa.gov/. (Accessed 28 January 2020).

Feng, P., Wang, W., Luo, J. J., et al. (2020). Using large-scale climate drivers to forecast meteorological drought condition in growing season across the Australian wheat belt. *Science of the Total Environment*, *724*, Article 138162.

Francois, C. (2015). Keras. Github. https://github.com/keras-team/keras.

Ganguli, P., & Reddy, M. J. (2014). Ensemble prediction of regional droughts using climate inputs and the SVM–copula approach. *Hydrological Processes*, *28*(19), 4989–5009.

Goodfellow, I., Bengio, Y., Courville, A., & Bengio, Y. (2016). *Deep learning*. MIT Press.

Haile, G. G., Tang, Q., Li, W., et al. (2020). Drought: Progress in broadening its understanding. *WIREs Water*, *7*(2), Article e1407.

Ham, Y., Kim, J., & Luo, J. (2019). Deep learning for multi-year ENSO forecasts. *Nature*, *573*, 568–572.

Han, P., Wang, P. X., Zhang, S. Y., & Zhu, D. H. (2010). Drought forecasting based on the remote sensing data using ARIMA models. *Mathematical and Computer Modelling*, *51*, 1398–1403.

Hanley, D. E., Bourassa, M. A., O'Brien, J. J., et al. (2003). A quantitative evaluation of ENSO indices. *Journal of Climate*, *16*, 1249–1258.

Hao, Z., Singh, V. P., & Xia, Y. (2018). Seasonal drought prediction: Advances, challenges, and future prospects. *Reviews of Geophysics*, *56*, 108–141.

Hao, Z., Yuan, X., Xia, Y., Hao, F., & Singh, V. P. (2017). An overview of drought monitoring and prediction systems at regional and global scales. *Bulletin of the American Meteorological Society*, *98*, 1879–1896.

Hayes, M., Svoboda, M., Le Comte, D., et al. (2005). *Drought monitoring: new tools for the 21st century*. Routledge: Taylor and Francis.

Hayes, M., Svoboda, M., Wall, N., & Widhalm, M. (2011). The Lincoln declaration on drought indices: universal meteorological drought index recommended. *Bulletin of American Meteorological Society*, *92*, 485–488.

Howden, M., Schroeter, S., Crimp, S., & Hanigan, I. (2014). The changing roles of science in managing Australian droughts: An agricultural perspective. *Weather and Climate Extremes*, *3*, 80–89.

Huang, B., L'Heureux, M., Lawrimore, J., et al. (2013). Why did large differences arise in the sea surface temperature datasets across the tropical Pacific during 2012? *Journal of Atmospheric and Oceanic Technology*, *30*, 2944–2953.

Kirono, D. G., Chiew, F. H., & Kent, D. M. (2010). Identification of best predictors for forecasting seasonal rainfall and runoff in Australia. *Hydrological Processes*, *24*, 1237–1247.

Krause, P., Boyle, D., & Bäse, F. (2005). Comparison of different efficiency criteria for hydrological model assessment. *Advances in Geosciences*, *5*, 89–97.

LeCun, Y., Bengio, Y., & Hinton, G. (2015). Deep learning. *Nature*, *521*, 436–444.

Lloyd-Hughes, B. (2014). The impracticality of a universal drought definition. *Theoretical and Applied Climatology*, *117*, 607–611.

Lundberg, S. M., & Lee, S. (2017). A unified approach to interpreting model predictions. In *Proceedings of the 31st international conference on neural information processing systems* (pp.4768–4777).

McKee, T. B., Doesken, N. J., & Kleist, J. (1993). The relationship of drought frequency and duration to time scales. In *Proceedings of the 8th conference on applied climatology* (pp. 179–184). CA, USA: Anaheim.

Mishra, A. K., & Desai, V. R. (2006). Drought forecasting using feed-forward recursive neural network. *Ecological Modelling*, *198*, 127–138.

Mishra, A. K., & Singh, V. P. (2011). Drought modeling–A review. *Journal of Hydrology*, *403*, 157–175.

Morid, S., Smakhtin, V., & Bagherzadeh, K. (2007). Drought forecasting using artificial neural networks and time series of drought indices. *International Journal of Climatology*, *27*, 2103–2111.

Morid, S., Smakhtin, V., & Moghaddasi, M. (2006). Comparison of seven meteorological indices for drought monitoring in Iran. *International Journal of Climatology*, *26*, 971–985.

Nash, J. E., & Sutcliffe, J. V. (1970). River flow forecasting through conceptual models part I—A discussion of principles. *Journal of Hydrology*, *10*, 282–290.

Naumann, G., Barbosa, P., Carrao, H., Singleton, A., & Vogt, J. (2012). Monitoring drought conditions and their uncertainties in Africa using TRMM data. *Journal of Applied Meteorology and Climatology*, *51*, 1867–1874.

Nicholls, N., Lavery, B., & Frederiksen, C. (1996). Recent apparent changes in relationships between the El Niño-Southern Oscillation and Australian rainfall and temperature. *Geophysical Research Letters*, *23*, 3357–3360.

Olah, C. (2015). Understanding lstm networks. http://colah.github.io/posts/2015-08-Understanding-LSTMs/.

Özger, M., Mishra, A. K., & Singh, V. P. (2012). Long lead time drought forecasting using a wavelet and fuzzy logic combination model: A case study in Texas. *Journal of Hydrometeorology*, *13*, 284–297.

Power, S., Delage, F. P., Chung, C. T., Ye, H., & Murphy, B. F. (2017). Humans have already increased the risk of major disruptions to Pacific rainfall. *Nature Communications*, *8*, 14368.

Pozzi, W., Sheffield, J., Stefanski, R., et al. (2013). Towards global drought early warning capability: Expanding international cooperation for the development of a framework for global drought monitoring and forecasting. *Bulletin of the American Meteorological Society*, *94*(6), 776–785.

Reichstein, M., Camps-Valls, G., Stevens, B., et al. (2019). Deep learning and process understanding for data-driven Earth system science. *Nature*, *566*, 195–204.

Ribeiro, M. T., Singh, S., & Guestrin, C. (2016). Why should I trust you? In *Proceedings of the 22nd ACM SIGKDD international conference on knowledge discovery and data mining* (pp. 1135–1144). New York: ACM.

Risbey, J. S., Pook, M. J., McIntosh, P. C., et al. (2009). On the remote drivers of rainfall variability in Australia. *Monthly Weather Review*, *137*(10), 3233–3253.

Shapley, L. S. (1953). A value for N-person games. Contributions to the theory of games. In Tucker A. W. Kuhn HW (Ed.), *Annals of mathematical studies* (pp. 307–317). Princeton: Princeton University Press.

Slette, I. J., et al. (2019). How ecologists define drought, and why we should do better. *Global Change Biology*, *25*, 3193–3200.

Stahl, K., & Demuth, S. (1999). *Methods for regional classification of streamflow drought series: Cluster analysis*: *Technical Rep 1*, ARIDE.

Ummenhofer, C. C., England, M. H., McIntosh, P. C., et al. (2009). What causes southeast australia's worst droughts?. *Geophysical Research Letters*, *46*(4), 1–5.

Van Dijk, A. I. J. M., Beck, H. E., Crosbie, R. S., et al. (2013). The millennium drought in Southeast Australia (2001–2009): Natural and human causes and implications for water resources, ecosystems, economy, and society. *Water Resources Research*, *49*(2), 1040–1057.

Van Loon, A. F., Glesson, T., Clark, J., et al. (2016). Drought in the anthropocene. *Nature Geoscience*, *9*, 89–91.

Vasiliades, L., Loukas, A., & Liberis, N. (2011). A water balance derived drought index for Pinios River Basin, Greece. *Water Resources Management*, *25*, 1087–1101.

Verdon-Kidd, D. C., & Kiem, A. S. (2009). Nature and causes of protracted droughts in southeast Australia: Comparison between the Federation, WWII, and Big Dry droughts. *Geophysical Research Letters*, *36*(22).

Vicente-Serrano, S. M., Quiring, S. M., Peña Gallardo, M., et al. (2020). A review of environmental droughts: Increased risk under global warming? *Earth Science Reviews*, *201*, Article 102953.

Woli, P., Jones, J., Ingram, K., & Paz, J. (2013). Forecasting drought using the agricultural reference index for drought (ARID): A case study. *Weather Forecast*, *28*, 427–443.

Yevjevich, V. M. (1967). Objective approach to definitions and investigations of continental hydrologic droughts. *Hydrology Papers*, (23).

Yihdego, Y., Vaheddoost, B., & Al-Weshah, R. A. (2019). Drought indices and indicators revisited. *Arabian Journal of Geosciences*, *12*, 69. http://dx.doi.org/10.1007/s12517-019-4237-z.